A Retention-Controlled Screening Framework for Chemical EOR in High-Temperature, High-Salinity Carbonate Reservoirs

Imad A. Adel[a], Alvaro Moralez[a], Emad W. Al-Shalabi[a,b],Waleed Alameri[a,b] Ali AlSumaiti[c], Shehadeh Masalmeh[c]

[a] *Chemical and Petroleum Engineering Department, Khalifa University of Science and Technology, Abu Dhabi, United Arab Emirates*

[b] *Research and Innovation Center on CO_2 and Hydrogen, Khalifa University of Science and Technology, Abu Dhabi, UAE*

[c] *Abu Dhabi National Oil Company (ADNOC), Abu Dhabi, United Arab Emirates*

* *Manuscript submitted to* ***Petroleum Exploration and Development*** *(KeAi Publishing).*

Abstract

Objective: High-temperature, high-salinity (HTHS) carbonates destabilize surfactants and elevate retention. This study develops a retention-controlled screening framework that links laboratory surfactant performance to field incremental recovery.

Methods: Thermal and aqueous stability tests, salinity-scan phase behavior with a Huh-correlation IFT cross-check, static and dynamic retention measurements, and surfactant-only coreflooding at 100 °C in outcrop and reservoir carbonates were integrated. Laboratory recovery was translated to RF_{inc} under explicit maturity and sweep assumptions and gated by C_{ret} at budget B_{max}.

Results: A GAC/IOS formulation was stable for 30 days at 120 °C, formed a Winsor III window between 30 000 and 60 000 ppm (S^* = 46 000 ppm), and gave $\sigma_{os} = 1.93 \times 10^{-3}$ mN·m^{-1} at 100 °C. Corefloods mobilized 76.1 % of S_{orw} at $k_w = 27.0 \times 10^{-3}$ μm^2 and 86.4 % at $k_w = 4.42 \times 10^{-3}$ μm^2; final retention was Γ = 0.16–0.17 mg·g^{-1}. The base case gave RF_{inc} = 25.9 % OOIP and C_{ret} = 5.69 USD/bbl, close to the B_{max} = 6 USD/bbl screening ceiling.

Conclusions: The framework satisfies the retention-cost gate with narrow margin under the stated assumptions. Retention reduction toward 0.10 mg·g^{-1} remains the main field-translation lever for this surfactant-only HTHS carbonate case.

Keywords: Chemical enhanced oil recovery; Carbonate reservoir; Surfactant flooding; Dynamic retention; Field screening

1. Introduction

Carbonate reservoirs host a major share of conventional oil resources and dominate many mature provinces in the Middle East [1-3]. Recovery from carbonates remains constrained by strong heterogeneity, fracture–matrix interaction, and mixed-to-oil wet surface chemistry, which limit waterflood displacement efficiency and increase residual oil saturation [4]. Chemical EOR targets microscopic displacement by modifying interfacial properties and rock–fluid interactions. Surfactant flooding reduces interfacial tension (IFT) and promotes mobilization of capillary-trapped oil, but carbonate systems impose stability and retention constraints under high-temperature and high-salinity (HTHS) conditions [5].

Reservoir temperatures frequently exceed 100 °C and approach 120 °C. Formation brines often exceed 150 000 ppm TDS with substantial hardness, which elevates precipitation risk and reduces the operational window of many surfactants. Carbonate surfaces trend toward mixed-to-oil wet states because of mineral surface charge, crude-oil polar components, and aging. Oil-wet behavior increases capillary trapping and elevates S_{orw} relative to typical water-wet sandstones [6]. HTHS conditions constrain surfactant stability and injectivity. Hydrolysis, salinity-driven precipitation, and microemulsion viscosity raise pressure drop and reduce effective transport. Formulations designed for seawater injections require stability margins along the in-situ salinity path and compatibility with divalent ions [7]. Chemical EOR is also positioned as a complement to CCUS-EOR in mature carbonate provinces where CO_2 injection faces miscibility limits, source-supply gaps, or surface-infrastructure constraints, particularly in offshore Middle Eastern fields where chemical-flooding pilots are progressing in parallel with CCUS feasibility studies [1].

A primary operational constraint for surfactant flooding in carbonates is chemical retention. Surfactant retention in carbonates directly increases chemical utilization and dominates project economics in many screening cases. Conventional anionic systems often exhibit multi-mg·g^{-1} retention in carbonates, while screening thresholds for field feasibility are commonly cited in the 0.1–0.2 mg·g^{-1} range [8]. To address this gap between typical performance and economic viability, it is necessary to identify the specific physical drivers of chemical loss. Fig. 1 illustrates the three primary mechanisms — electrostatic adsorption, phase trapping, and precipitation — that collectively drive high surfactant consumption in HTHS carbonate environments. Phase trapping increases when the microemulsion is oil-continuous (Winsor II) because surfactant partitions into the oil-rich microemulsion and is retained with trapped oil or trapped microemulsion during the aqueous chase [9].

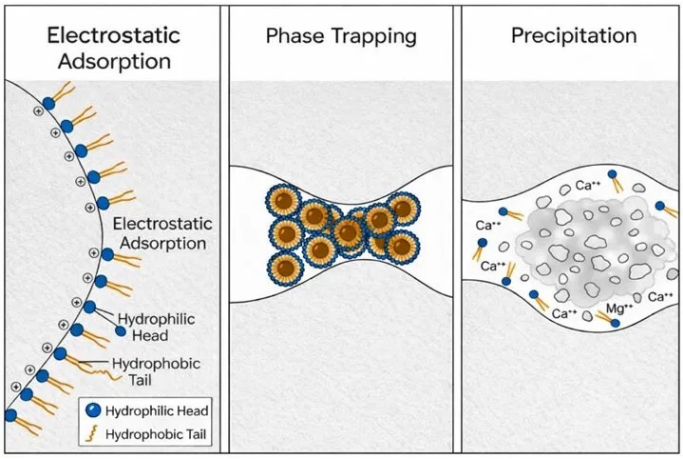

Fig. 1. Primary retention mechanisms in carbonate reservoirs: (a) electrostatic adsorption of anionic surfactant heads to positively charged calcite sites; (b) phase trapping within the Winsor Type II regime; (c) precipitation induced by divalent cations in high-salinity brine.

Sulfate-based surfactants frequently degrade at elevated temperatures and hardness because of hydrolysis and precipitation in high-salinity brines. Internal olefin sulfonates (IOS) extend salinity and temperature tolerance and usually achieve low IFT, but retention and stability in carbonates remain constraints at HTHS. Guerbet alkoxy carboxylates (GACs) offer improved thermal stability and reduced adsorption owing to their bulky branched hydrophobe and tunable EO/PO architecture [10, 11]. Table 1 summarizes key properties and performance tradeoffs among sulfate-based surfactants, IOS, and GACs relevant to carbonate chemical EOR. The parameter ranges reflect variance across crude oils, brines, and mineralogies; they serve strictly as screening guidelines.

Table 1. Screening-level comparison of anionic surfactant classes in carbonate brines containing divalent ions. Parameters represent typical reported operational ranges.

Property / performance metric	**Sulfate-based surfactants**	**Sulfonate-based surfactants (IOS)**	**Carboxylate-based surfactants (GAC)**
Thermal stability (°C)	≤ 60 (limited by hydrolysis)	90–100 (moderate stability)	≥ 120 (excellent stability)
Salinity tolerance (ppm TDS)	Moderate (< 50 000)	Good (50 000–150 000)	Excellent (> 150 000)
Hardness tolerance (Ca^{2+}, Mg^{2+})	Limited (precipitates readily)	Moderate (possible precipitation)	High (minimal precipitation risk)
IFT reduction capability ($mN \cdot m^{-1}$)	Good (10^{-2} to 10^{-3})	Good (10^{-2} to 10^{-3})	Excellent (10^{-3} to 10^{-4})
Adsorption and retention	High (> 2 $mg \cdot g^{-1}$)	Moderate (0.5–2 $mg \cdot g^{-1}$)	Low (0.1–0.5 $mg \cdot g^{-1}$)

Data sources: [7, 11, 22, 21].

Formulation design in seawater-injection carbonates often involves blending a primary surfactant with co-surfactants and co-solvents to tune optimum salinity, widen the Winsor Type III window, and manage microemulsion viscosity. Carbonate coreflood studies report high displacement efficiencies using GAC and IOS-based formulations, often within SP and ASP designs [11, 12, 13, 14]. Gaps persist between published coreflood datasets and the specific petrophysical and thermodynamic constraints of low-permeability, high-temperature carbonate reservoirs. Many studies utilize high-permeability cores at moderate temperatures or employ polymer and alkali to provide mobility control, which obscures the isolated surfactant displacement efficiency and omits injectivity impairment risks in tight matrices [15, 16]. Evaluations below 85 °C also fail to capture the stability and retention constraints inherent to 100 °C reservoirs, and historical datasets frequently omit the dynamic retention metrics required for economic scaling [13, 17]. This study addresses these gaps through an integrated laboratory program centered on a screened surfactant-only GAC and IOS formulation (designated SF4) designed for seawater injection at 100 °C. The objectives of this study are:

(1) Screen a GAC and IOS blend for 100 °C and seawater salinity (43 373 ppm) with stability screening at 120 °C.

(2) Quantify phase behavior, interfacial tension, and wettability response under high-temperature conditions aligned with seawater-injection constraints.

(3) Quantify static adsorption and dynamic retention and interpret both within a consistent mass-balance framework.

(4) Evaluate surfactant-only displacement in outcrop carbonate and low-permeability reservoir carbonate core at 100 °C.

(5) Translate retention and S_{orw}-based recovery into field-screening metrics using explicit maturity and sweep assumptions.

2. Materials and methods

2.1. Materials

2.1.1. Surfactants and chemicals

The formulations used anionic surfactants selected for high-temperature, high-salinity service. Two IOS surfactants (IOS15–18 and IOS20–24) were used as co-surfactants to tune phase behavior and shift optimum salinity toward seawater-relevant values. An ethoxylated phenol co-solvent was included in all formulations to reduce interfacial rigidity, improve stability, and lower microemulsion viscosity. Surfactants and the co-solvent were obtained from commercial suppliers. Fig. 2 summarizes representative structures and labeled domains used in this study. All surfactant and co-solvent concentrations reported in this work are on an active-matter basis.

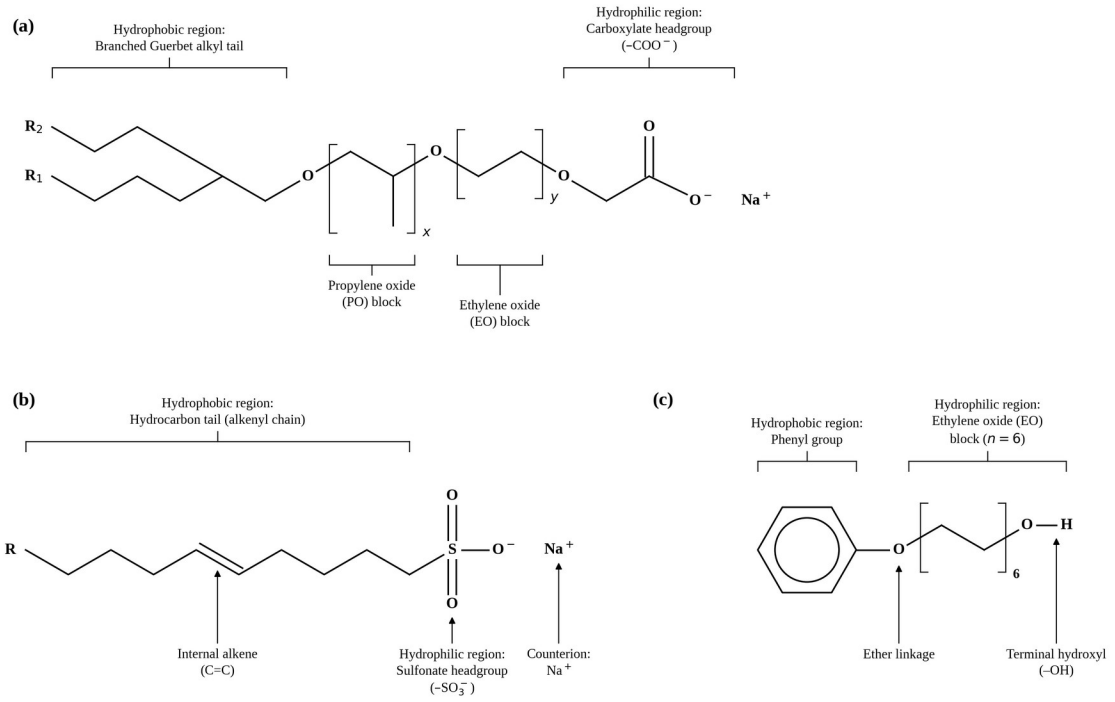

Fig. 2. Representative amphiphile structures used in this study: (a) Guerbet alkoxy carboxylate (GAC, sodium salt); (b) internal olefin sulfonate (IOS, sodium salt); (c) ethoxylated phenol co-solvent.

Following initial screening, five formulations (SF0 to SF4, Table 2) were selected for detailed evaluation. The primary variables were the GAC hydrophobe and the IOS blend. SF0 served as the baseline formulation, while SF4 represents the down-selected blend. SF4 used C28–GAC as the primary surfactant, with IOS co-surfactants, to achieve 1.0 wt % total active surfactant. An ethoxylated phenol co-solvent was added at 0.5 wt % to improve microemulsion phase behavior and reduce equilibration time.

Table 2. Composition of the evaluated surfactant formulations (SF0–SF4) on an active-matter weight basis.

Formulation	Composition
SF0	0.5 wt % C28-45PO-45EO-COONa + 0.5 wt % IOS15
SF1	0.5 wt % C13-35PO-30EO-COONa + 0.25 wt % IOS15 + 0.25 wt % IOS20
SF2	0.5 wt % C18-35PO-30EO-COONa + 0.25 wt % IOS15 + 0.25 wt % IOS20
SF3	0.5 wt % C24-35PO-30EO-COONa + 0.25 wt % IOS15 + 0.25 wt % IOS20
SF4	0.5 wt % C28-45PO-45EO-COONa + 0.25 wt % IOS15 + 0.25 wt % IOS20

2.1.2. Brines and crude oil

Synthetic brines were prepared to replicate the target high-salinity formation waters (FW1 and FW2) and the injection seawater (SW). Injection seawater has a TDS of 43 373 ppm. Tables 3 and 4 summarize key properties and ionic compositions of these synthetic brines. Stock-tank crude oil from the target reservoir was provided by the operator. The crude was filtered and degassed before use and has an API gravity of approximately 35°. Oil viscosity was measured at 25 °C and 50 °C, yielding values of 5.84 mPa·s (5.84 cP) and 2.34 mPa·s (2.34 cP), respectively.

Table 3. Properties and ionic composition of synthetic formation water (FW) and injection seawater (SW).

Property	FW1	FW2	SW
Total dissolved solids (ppm)	167 301	243 028	43 373
Hardness (ppm as $CaCO_3$)	10 696	26 520	2 122
Viscosity (mPa·s)	1.52	1.57	1.02
Density ($g \cdot cm^{-3}$)	1.16	1.17	1.04

Density and viscosity values were measured at ambient conditions.

Table 4. Ionic composition of synthetic brines ($mg \cdot L^{-1}$).

Ion	FW1	FW2	SW
Na^+	52 952	66 130	13 662
Ca^{2+}	9 250	23 246	539
Mg^{2+}	1 446	2 674	1 583
K^+	744	—	498
Cl^-	102 916	150 675	27 092
SO_4^{2-}	0	230	0
HCO_3^-	0	—	0
Br^-	0	—	0
I^-	0	—	0
TDS (ppm)	167 114	243 028	43 373

2.1.3. Rock samples

Two carbonate core plugs were used to evaluate formulation performance across distinct permeabilities and rock types. Core-1 is an outcrop Indiana limestone, and Core-2 is a reservoir carbonate core. Table 5 summarizes core petrophysical properties and saturation endpoints.

Table 5. Petrophysical properties and saturation endpoints of the evaluated carbonate core plugs.

ID	Lithology	ϕ (%)	k_w / 10^{-3} µm^2	$k_{w,Sorw}$ / 10^{-3} µm^2	S_{wi} (%)	S_{orw} (%)
Core-1	Indiana limestone	18.2	27.0 (27.0 mD)	21.7	28.5	30.1
Core-2	Reservoir carbonate	22.0	4.42 (4.42 mD)	2.03	16.0	40.0

Absolute permeability is reported as k_w. Effective water permeability after waterflood is reported as $k_{w,Sorw}$ at S_{orw}. mD value shown in parentheses on first use only (PED house style).

2.2. Experimental procedures

2.2.1. Thermal and aqueous stability assessment

Thermal stability was evaluated by aging formulations prepared in seawater in sealed glass ampoules at 120 °C for 30 days. Stability was assessed by visual inspection for turbidity, phase separation, precipitation, and color change. Aqueous stability limits were determined at 100 °C by incrementally increasing brine salinity until persistent turbidity was observed. The measured 75 000 ppm aqueous stability limit requires a seawater pre-flush. The dispersive mixing zone between the pre-flush and high-salinity formation water creates a salinity gradient that must be managed to prevent surfactant precipitation at the leading edge of the chemical slug [18].

2.2.2. Phase behavior

Phase behavior was characterized using standard salinity-scan experiments. Equal volumes of surfactant solution and crude oil were mixed in sealed pipettes and aged at 100 °C for two weeks to reach equilibrium. Phase volumes were recorded and used to identify the microemulsion type (Winsor I, II, or III). Solubilization ratios for oil and water were computed to define the characteristic solubilization ratio at optimum salinity (R^*). Oil and water solubilization ratios are defined in Eqs. (1) and (2):

$$R_o = V_o / V_s \quad (1)$$

$$R_w = V_w / V_s \quad (2)$$

where V_o and V_w are the volumes of oil and water solubilized in the middle-phase microemulsion, and V_s is the volume of active surfactant solubilized in the middle phase. The characteristic solubilization ratio at optimum salinity is denoted R^*.

2.2.3. Interfacial tension

Interfacial tension between crude oil and surfactant formulations was measured using spinning-drop tensiometry to quantify ultra-low IFT and pendant-drop tensiometry to measure baseline IFT. Spinning-drop measurements [19] were acquired between 60 °C and 90 °C because of equipment thermal limits, and the values were extrapolated to 100 °C using a power-law regression. IFT at optimum salinity was also estimated using the Huh correlation [20] to provide an independent cross-check (Eq. (3)).

$$\sigma^* = C_{Huh} / (R^*)^2 \quad (3)$$

where σ^* is the IFT at optimum salinity, C_{Huh} is a constant (typically 0.3 $mN \cdot m^{-1}$), and R^* is the characteristic solubilization ratio at optimum salinity. The baseline IFT between crude oil and seawater without surfactant was measured by pendant-drop tensiometry and averaged 21.5 $mN \cdot m^{-1}$.

2.2.4. Wettability

For each measurement, an oil-aged carbonate chip was submerged in either seawater or SF4. An oil droplet was dispensed onto the submerged rock surface and imaged for contact-angle determination using instrument software. Each condition was repeated three times, and the reported values represent the average. These ambient-condition tests provide qualitative, screening-level indications of surfactant-induced surface modification; they do not establish in-situ wettability or quantify relative-permeability shifts at reservoir temperature and pressure.

2.2.5. Static adsorption and dynamic retention

Static adsorption tests were used to quantify equilibrium adsorption on carbonate substrates. Crushed-rock substrates were sieved to the 75–150 μm size fraction (retained on the 100-mesh sieve and passing the 200-mesh sieve) and equilibrated for 24 h under agitation to promote equilibrium. The same size fraction was used for the Indiana limestone substrate and for the reservoir carbonate substrate, except where noted in §3.3.1. Adsorption is reported on a mass-normalized basis ($mg \cdot g^{-1}$) by material balance, consistent with common static-adsorption practice in surfactant EOR [21]. The tests were conducted at 25 °C and 100 °C for 24 h under agitation. Following equilibration, solids were separated by centrifugation, and the supernatant was analyzed to determine the equilibrium concentration. Static adsorption (Γ_s) in $mg \cdot g^{-1}$ is defined by material balance (Eq. (4)).

$$\Gamma_s = [(C_0 - C_{eq}) \cdot V] / m_{rock} \quad (4)$$

In Eq. (4), C_0 and C_{eq} are the initial and equilibrium surfactant concentrations (ppm) in the static-adsorption test, V is the aqueous-solution volume (L), and m_{rock} is the dry rock mass (g).

Dynamic retention during coreflooding was quantified by material balance using effluent surfactant-concentration histories and injected volumes (Eq. (5)).

$$\Gamma = (1 / m_{rock}) \cdot [\, minj - \int 0V\_inj\, C_{eff}\, dV \,] \quad (5)$$

In Eq. (5), V_{inj} is the injected aqueous volume and C_{eff} is the effluent surfactant concentration. Concentrations expressed in ppm are taken as numerically equivalent to $mg \cdot L^{-1}$; this equivalence is exact within ≤0.5 % for the dilute aqueous phase relevant to surfactant slugs (active-matter content ≤1.0 wt %) at the carrier-phase density of the seawater-salinity injection brine. The integral represents the produced surfactant mass with unit-consistent volume conversion. The salinity-gradient post-flush correction accounts for desorbed surfactant and improves the estimation of net retained mass. Surfactant concentrations in effluent samples were quantified using high-performance liquid chromatography (HPLC) coupled to an evaporative light-scattering detector (ELSD). Separation was performed on a C18 reversed-phase column (150 mm × 4.6 mm, 5 μm particle size) at 40 °C, with a flow rate of 1.0 $mL \cdot min^{-1}$ and an injection volume of 20 μL. The mobile phase consisted of (A) water with 0.1 % formic acid and (B) acetonitrile with 0.1 % formic acid, run as a linear gradient from 30 % B to 95 % B over 12 min, held at 95 % B for 3 min, and re-equilibrated for 5 min. The ELSD drift tube was held at 60 °C with a nebulizer gas flow of 1.6 $L \cdot min^{-1}$. Calibration curves were prepared using SF4 standards over 0–5 000 ppm (8-point ladder, log-log fit, $R^2 \geq 0.995$). The limit of quantification (LOQ) was 50 ppm, determined as 10 × the baseline noise of solvent blanks. Replicate injections of three calibration standards gave relative standard deviations below 3.5 % across the working range.

2.2.6. Dynamic coreflooding

Dynamic corefloods were performed using a high-pressure, high-temperature coreflooding system with a core holder rated to 34.5 MPa (5 000 psi) confining pressure and an oven rated to 200 °C.

Corefloods were conducted at 100 °C and a constant confining pressure of 6.9 MPa (1 000 psi) and a back-pressure of 1.4 MPa (200 psi) to maintain single-phase flow. Flow rate was fixed at 0.25 $cm^3 \cdot min^{-1}$ for all stages. Flow remained in a laminar, viscous-dominated regime ($R_e < 1$). The Reynolds number was computed as $R_e = \rho v D/\mu$ with superficial velocity v = Q/A, brine density ρ, viscosity μ, and core diameter D. With D = 3.77 cm, Q = 0.25 $cm^3 \cdot min^{-1}$, ρ = 1.016 $g \cdot cm^{-3}$, and μ = 0.4 mPa·s, $R_e \approx 0.36$ in both floods. Viscous forces therefore dominate over inertial forces, the pressure drop scales linearly with the rate, and Darcy-flow interpretations remain valid for trends in injectivity and resistance factors.

The flooding sequence consisted of the following steps:

(1) Core preparation and aging: cores were cleaned, dried, vacuum-saturated with formation water, flooded with crude oil to establish initial oil saturation, and aged at 100 °C for two weeks.

(2) S_{orw} establishment and seawater conditioning: S_{orw} was established by centrifuge before chemical injection. 5 PV of seawater at 100 °C were then injected to establish baseline pressure response and to condition the core to near-seawater salinity before SF4 injection.

(3) Surfactant injection: SF4 (1.0 wt % active surfactant with 0.5 wt % co-solvent) was injected at seawater salinity until the oil cut reached zero. Effluent was collected in successive fractions of 0.05 PV; the oil cut for each fraction was computed by volumetric phase separation. The endpoint was defined as three consecutive fractions (covering a 0.15 PV sampling window) in which the measured oil cut was at or below the detection threshold of 0.5 % (v/v). The slug PV reported below corresponds to the cumulative injected volume at the start of the first of these three fractions. This endpoint required 0.8 PV in Core-1 and 1.0 PV in Core-2.

(4) Salinity-gradient post-flush: a multi-step post-flush was injected from 43 373 ppm to 20 000 ppm to 10 000 ppm TDS.

Pressure response was interpreted using the resistance factor (Eq. (6)).

$$F_r = \Delta P / \Delta P_{baseline} \quad (6)$$

where $\Delta P_{baseline}$ is the differential pressure during seawater injection at the same flow rate.

Microscopic displacement efficiency at the pore scale is governed by the capillary number, which expresses the ratio of viscous to capillary forces. The capillary number is reported here for both corefloods as a screening indicator for the operating regime relative to the trapping-curve plateau (Eq. (7)).

$$N_c = \mu v / \sigma \quad (7)$$

where μ is the dynamic viscosity of the displacing aqueous phase (Pa·s), v is the Darcy (superficial) velocity ($m \cdot s^{-1}$), and σ is the oil–surfactant interfacial tension ($N \cdot m^{-1}$). For ultra-low IFT formulations, N_c typically exceeds the trapping-curve plateau (~10^{-5}–10^{-4}) reported for water-wet systems, supporting effective microscopic mobilization.

3. Results and discussion

3.1. Formulation screening: stability, phase behavior, and IFT

The formulation screening aimed to identify a surfactant blend capable of achieving and maintaining ultra-low interfacial tension under 100 °C seawater-injection conditions. The screening targeted ultra-low IFT at seawater salinity while preserving operational stability along the in-situ salinity path created by dispersion and mixing. The screening criteria were thermal stability, practical phase behavior with a Winsor Type III window, and IFT values in the 10^{-3} $mN \cdot m^{-1}$ range.

3.1.1. Stability constraints and operational windows

For thermal stability, all solutions remained clear, exhibiting a single phase with no precipitation or color change after aging in seawater at 120 °C for 30 days. This demonstrates the thermal stability of the GAC and IOS structures against hydrolysis and thermal degradation under the tested conditions [10].

Aqueous stability at 100 °C imposes the primary operational constraint for seawater injection into higher-salinity formation water. Table 6 summarizes aqueous stability limits, phase-behavior metrics, and IFT performance at 100 °C for SF0 to SF4. SF0 initially exhibited an optimum salinity of 88 kppm TDS, significantly higher than the intended injection salinity. SF0 and SF4 share the same 0.5 wt % primary GAC, but they differ in the IOS blend used to tune salinity. SF0 used 0.5 wt % lower-chain IOS as the co-surfactant, whereas SF4 used a split blend of 0.25 wt % lower-chain IOS and 0.25 wt % higher-chain IOS. Introducing the higher-chain IOS progressively shifted the optimum salinity downward, reducing it from 88 kppm TDS (SF0) to about 46 kppm TDS (SF4), which aligns closely with the seawater-injection salinity path. This behavior is consistent with reports that IOS co-surfactants can lower optimum salinity and broaden practical operating windows by tuning microemulsion curvature and salinity tolerance [22].

Table 6. Aqueous stability, phase behavior, and interfacial tension (IFT) metrics for formulations SF0–SF4 at 100 °C.

Formulation	Aqueous stability (ppm TDS)	Middle-phase range (ppm TDS)	S^* (ppm TDS)	R^* ($cm^3 \cdot cm^{-3}$)	σ^* ($mN \cdot m^{-1}$)	σ_{os} ($mN \cdot m^{-1}$)
SF0	105 000	85 000 to 95 000	88 400	9.0	3.62×10^{-3}	2.50×10^{-2}
SF1	50 000	20 000 to 45 000	37 000	7.0	6.12×10^{-3}	4.20×10^{-3}
SF2	60 000	30 000 to 45 000	40 000	9.0	3.70×10^{-3}	2.58×10^{-3}
SF3	70 000	30 000 to 50 000	45 000	9.5	3.32×10^{-3}	3.07×10^{-3}
SF4	75 000	30 000 to 60 000	46 000	12.0	2.08×10^{-3}	1.93×10^{-3}

S^* is optimum salinity, R^* is the solubilization ratio at S^*, σ^* is Huh-correlation IFT computed at S^*, and σ_{os} is spinning-drop IFT measured at seawater salinity (43 373 ppm TDS) extrapolated to 100 °C.

SF4 exhibited an aqueous stability limit of 75 000 ppm TDS. The aqueous stability limit provides a buffer of 30 000 ppm above the injection brine salinity, so that modest salinity and hardness excursions along the mixing path do not trigger precipitation during slug preparation and early propagation [5]. This limit exceeds seawater salinity and supports seawater injection, but it does not cover direct contact with formation brines at 167 301 ppm or 243 028 ppm TDS. Field translation requires a seawater pre-flush to prevent direct contact between the formulation and formation water along the dispersive mixing zone.

Among SF1 to SF4, SF4 provides the largest stability margin above seawater, the broadest Winsor Type III window, and the highest R^*. This combination improves tolerance to dispersive salinity gradients during slug propagation and reduces precipitation risk under realistic mixing. SF3 served as an alternative formulation because it met the phase-behavior and IFT targets near seawater while maintaining an acceptable stability margin.

3.1.2. Phase behavior

Phase-behavior screening targeted an optimum salinity near seawater and a high solubilization ratio to support ultra-low IFT with injectivity control. The comparison between SF0 and SF4 shows the blending effect. SF0 exhibited S^* = 88 400 ppm TDS, exceeding seawater salinity. SF4 shifted S^* downward to 46 000 ppm TDS through the IOS15–18 and IOS20–24 co-surfactant blend. SF4 formed a broad Winsor Type III window from 30 000 to 60 000 ppm TDS, which increases tolerance to salinity gradients during slug propagation. Fig. 3 summarizes the screening space by linking S^* and R^* to aqueous stability limits across SF1 to SF4.

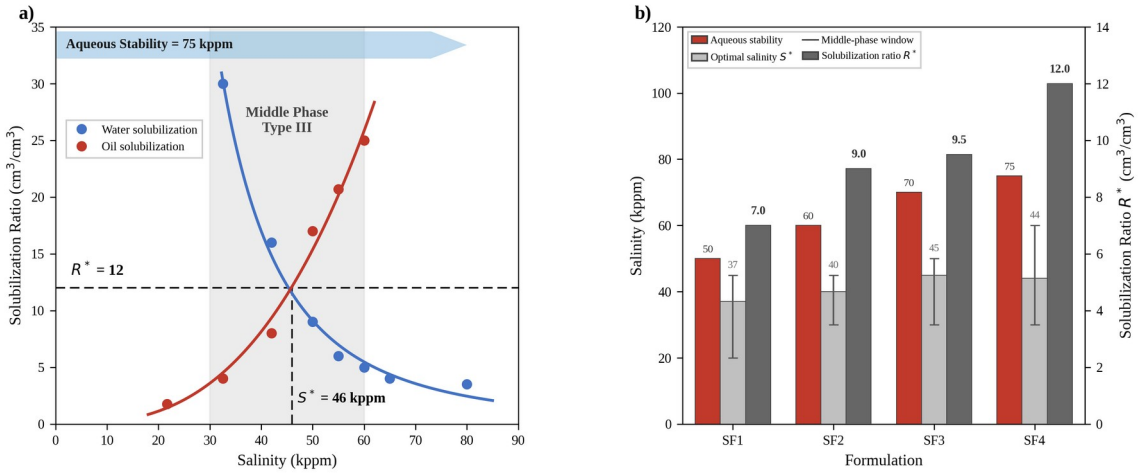

Fig. 3. Formulation screening map linking aqueous stability, optimum salinity, and solubilization capacity: (a) determination of solubilization parameters for formulation SF4; (b) evolution of S^* and R^* versus aqueous-stability limit across formulations SF1–SF4.

For SF0, σ_{os} = 2.50 × 10^{-2} mN·m^{-1} is an order of magnitude higher than σ^* = 3.62 × 10^{-3} mN·m^{-1} (Table 6). This discrepancy is consistent with SF0 being well off-optimum at seawater salinity: SF0 has S^* = 88 400 ppm TDS, whereas seawater salinity is 43 373 ppm TDS. The Huh correlation is defined at optimum salinity; applying it predicts the IFT minimum at S^*, while the spinning-drop measurement at seawater salinity samples the IFT well below S^* on the Winsor I side of the phase diagram, where IFT rises steeply away from the optimum. SF4, in contrast, has S^* = 46 000 ppm TDS, essentially coincident with seawater salinity, so σ_{os} and σ^* agree to within 10 %. The SF0 result therefore illustrates a salinity-mismatch artifact rather than a failure of the Huh correlation.

3.1.3. Ultra-low IFT and Huh-correlation cross-check

The IFT of SF4 at seawater salinity was determined from spinning-drop measurements acquired between 60 and 90 °C and extrapolated to 100 °C (Fig. 4). The extrapolated IFT for SF4 at 100 °C at seawater salinity was σ_{os} = 1.93 × 10^{-3} mN·m^{-1}. The Huh correlation with C_{Huh} = 0.3 mN·m^{-1} and R^* = 12 yields σ^* = 2.08 × 10^{-3} mN·m^{-1} for SF4. σ^* aligns with σ_{os} for SF4 because seawater salinity (43 373 ppm TDS) closely matches S^* (46 000 ppm TDS). Baseline IFT between crude oil and seawater without surfactant averaged 21.5 mN·m^{-1} under ambient pendant-drop conditions.

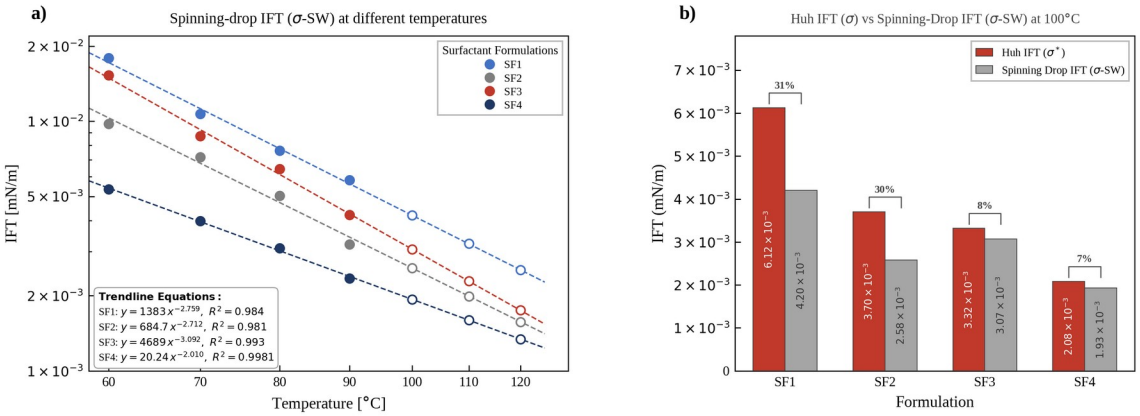

Fig. 4. Interfacial-tension behavior of formulations SF1–SF4: (a) spinning-drop IFT versus temperature at seawater salinity (σ_{os}) with extrapolation to 100 °C; (b) comparison of Huh-correlation IFT at optimum salinity (σ^*) versus spinning-drop IFT at seawater salinity (σ_{os}) at 100 °C.

3.2. Wettability response (ambient screening)

Wettability states are commonly interpreted from the water-phase contact angle, where water-wet corresponds to $\theta < 75°$, intermediate-wet to $75° \leq \theta \leq 105°$, and oil-wet to $\theta > 105°$ [23]. Fig. 5 summarizes the ambient-condition contact-angle response of oil-aged carbonate chips from the outcrop and reservoir rock exposed to seawater and SF4. The chip contact angle shifted from strongly oil-wet (161°, 171°) toward intermediate-wet (69°, 72°) after SF4 exposure. This shift provides qualitative evidence of rock-surface modification under the same measurement protocol.

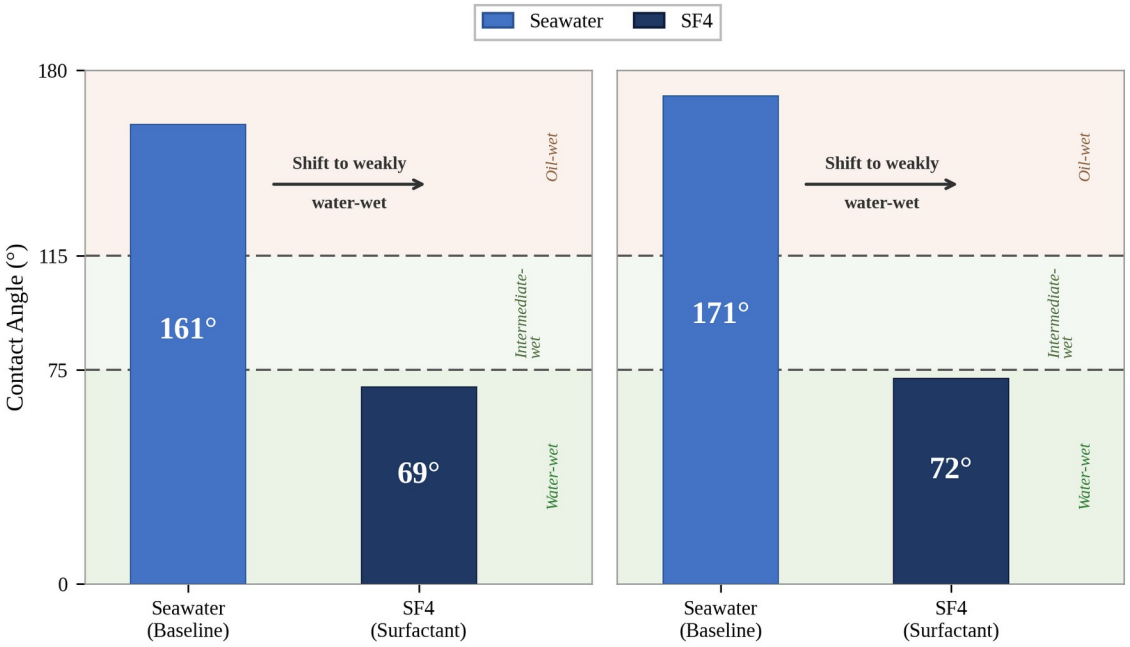

Fig. 5. Ambient-condition contact-angle measurements of oil-aged carbonate chips in seawater and SF4: (a) Indiana limestone; (b) reservoir carbonate.

The wettability shift is consistent with surfactant-induced surface modification on carbonate. The dataset does not include advancing and receding angles or surface spectroscopy, so contact-angle hysteresis and the underlying adsorption configuration remain unresolved. These ambient measurements provide qualitative evidence of wettability alteration only; they do not establish in-situ wettability at 100 °C and reservoir pressure.

3.3. Surfactant retention

Surfactant retention governs chemical utilization and directly shapes field-screening outcomes. This work quantified retention using both static adsorption on crushed substrates and dynamic material balance during coreflooding.

3.3.1. Static adsorption

Static adsorption was used as an initial screening metric to rank formulations for carbonate retention risk before committing to coreflooding. SF3 and SF4 were both identified as top candidates during phase-behavior screening, so static adsorption served as an additional discriminator for formulation selection.

Temperature reduced adsorption for both formulations. Adsorption decreased from 25 °C to 100 °C on both substrates, which aligns with published carbonate adsorption datasets reporting lower surfactant adsorption density at elevated temperature owing to weaker net adsorption affinity and enhanced desorption kinetics [24]. At both temperatures, adsorption on the reservoir carbonate powder was slightly lower than on Indiana limestone (for SF4: 1.08 versus 1.20 $mg \cdot g^{-1}$ at 25 °C; 0.78 versus 0.87 $mg \cdot g^{-1}$ at 100 °C). This rock-type comparison remains qualitative because the crushed-rock size fractions were not identical, and particle size affects accessible surface area and apparent adsorption. The formulation ranking remained unchanged across temperature and substrate, indicating a consistent formulation-level difference in net adsorption affinity across the tested conditions.

3.3.2. Dynamic retention

Dynamic retention was calculated during the corefloods from injected and produced surfactant masses using effluent concentration histories. Immediately after surfactant-slug injection, retention was 0.23 $mg \cdot g^{-1}$ for Core-1 and 0.21 $mg \cdot g^{-1}$ for Core-2. After the salinity-gradient post-flush, final retentions were 0.16 $mg \cdot g^{-1}$ for Core-1 and 0.17 $mg \cdot g^{-1}$ for Core-2.

The multi-step salinity-gradient post-flush reduced net retained surfactant mass relative to the immediate post-slug condition. The desorbed surfactant mass recovered during the post-flush, relative to the retained mass measured immediately after slug injection, was 30.4 % for Core-1 (Γ decreased from 0.23 to 0.16 $mg \cdot g^{-1}$) and 19.0 % for Core-2 (Γ decreased from 0.21 to 0.17 $mg \cdot g^{-1}$). The material balance closes within ±5 % for both corefloods, where the closure is computed as (injected SF4 mass) − (effluent SF4 mass) − (retained SF4 mass on rock) divided by injected SF4 mass; the residual is within the combined uncertainty of the HPLC-ELSD measurement, the integration of the effluent history, and the dry-rock mass. Lowering ionic strength weakens ion-screening and cation-bridging effects that promote adsorption in saline and hard brines, increasing the fraction of reversibly retained surfactant that can desorb during the chase [25]. Negative-salinity-gradient designs, where the chase is under-optimum relative to the slug, have been shown to reduce surfactant loss by promoting partitioning back toward the aqueous phase and extending favorable phase behavior during propagation [26]. The laboratory stepwise gradient provides a strong local desorption driving force. At the field scale, dispersion and crossflow broaden salinity transitions, which reduces desorption driving force and increases effective retention relative to sharp laboratory step changes [5, 27].

Comparing static and dynamic retentions shows that static tests on crushed rock typically overestimate the retention observed in dynamic corefloods. This discrepancy arises because crushed grains expose a higher surface area than intact rock, and static tests also omit oil and flow-path effects [21]. The two measurements are reported as complementary.

3.4. Coreflooding performance

Two dynamic coreflooding experiments evaluated SF4 performance at 100 °C in an outcrop Indiana-limestone carbonate (Core-1) and a Middle East reservoir carbonate core (Core-2). The conditions applied were 100 °C, 1.4 MPa (200 psi) back-pressure, an injection rate of 0.25 $cm^3 \cdot min^{-1}$, and a PV axis offset of 5 PV of seawater pre-flush injection. The sequence consisted of 5 PV seawater pre-flush, SF4 injection at seawater salinity to zero oil cut (0.8 PV in Core-1 and 1.0 PV in Core-2), followed by a stepwise salinity-gradient post-flush (43 373 → 20 000 → 10 000 ppm TDS). The results are summarized in Table 7.

Table 7. Summary of dynamic coreflooding parameters and recovery endpoints for formulation SF4 at 100 °C.

Core ID	k_w / 10^{-3} µm²	S_{orw} (%)	Slug size (PV)	Recovery of S_{orw} (%)	S_{orc} (%)	Γ ($mg \cdot g^{-1}$)
Core-1 (outcrop)	27.0	30.1	0.8	76.1	7.20	0.16
Core-2 (reservoir)	4.42	40.0	1.0	86.4	5.43	0.17

Slug size denotes the PV at which oil cut equals zero. Γ denotes final dynamic retention after the salinity-gradient post-flush.

3.4.1. Core-1 (moderate-permeability outcrop)

The Core-1 coreflood evaluated performance in a moderate-permeability carbonate system. Fig. 6 reports oil saturation, tertiary recovery, and differential pressure versus cumulative PV injected.

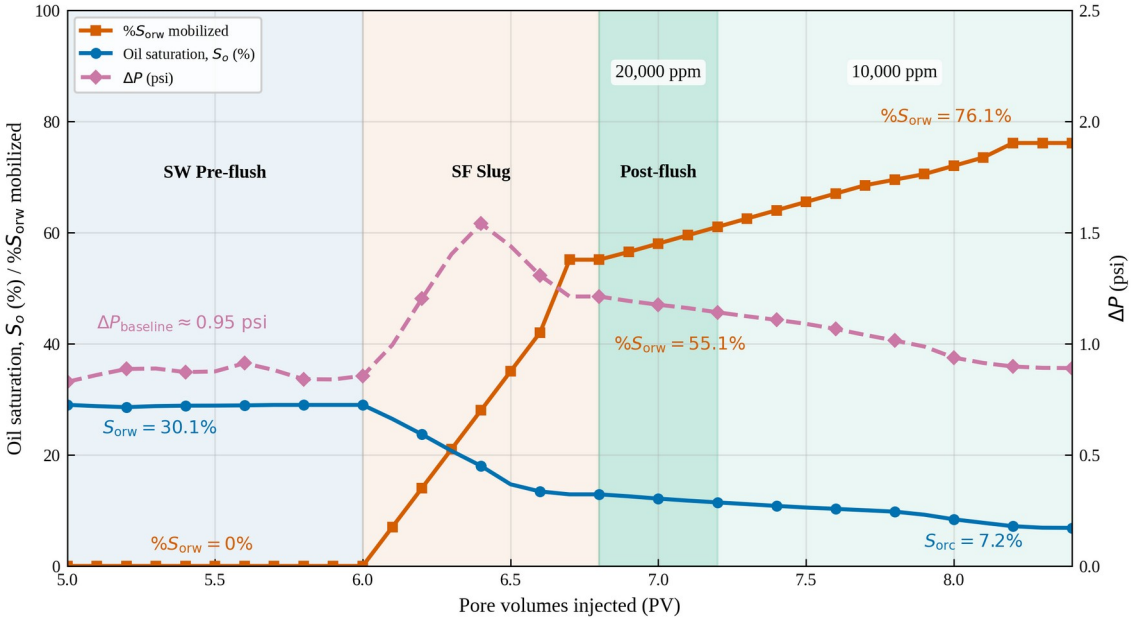

Fig. 6. Dynamic coreflooding response for Core-1 (Indiana limestone) at 100 °C: oil saturation, tertiary recovery, and differential pressure versus injected pore volumes (PV).

Waterflood and conditioning. The centrifuge established S_{orw} = 30.1 % before chemical injection. Seawater injection then provided a baseline pressure response. A 5 PV seawater pre-flush conditioned the core to near-seawater salinity before the chemical slug. This laboratory conditioning volume targets brine uniformity and differs from field pre-flush sizing. Figs. 6 and 8 plot injected PV with a 5-PV offset to zoom on the chemical and post-flush stages.

Surfactant slug injection. SF4 was injected at seawater salinity until the oil cut reached zero at 0.8 PV. Oil mobilization began after 0.1 PV of surfactant injection. Oil saturation decreased from 30.1 to 13.5 % by the end of the slug. Cumulative mobilization during the slug reached 55.1 % of S_{orw}.

Pressure dynamics. Differential pressure increased and reached 11.7 kPa (1.70 psi) at 6.4 PV injected. Baseline differential pressure during seawater injection averaged 6.5 kPa (0.95 psi). Core-1 reached a peak resistance factor of F_r = 1.79. The capillary number during SF4 injection, computed from Eq. (7) using μ = 1.02 mPa·s (seawater carrier), v = 3.73 × 10^{-6} m·s^{-1}, and σ_{os} = 1.93 × 10^{-3} mN·m^{-1}, is N_c ≈ 2.0 × 10^{-3}, well above the trapping-curve plateau (~10^{-5}–10^{-4}) reported for water-wet sandstone systems and consistent with effective microscopic mobilization at ultra-low IFT.

Post-flush. The salinity-gradient post-flush increased total tertiary recovery to 76.1 % of S_{orw} at 8.2 PV injected. The residual oil saturation after the chemical flood was S_{orc} = 7.20 %. Differential pressure returned to near-baseline, indicating no sustained impairment in this core.

3.4.2. Core-2 (low-permeability reservoir carbonate)

The Core-2 coreflood evaluated performance in the low-permeability reservoir rock at S_{orw} = 40.0 %. Fig. 7 reports oil saturation, tertiary recovery, and differential pressure versus cumulative PV injected.

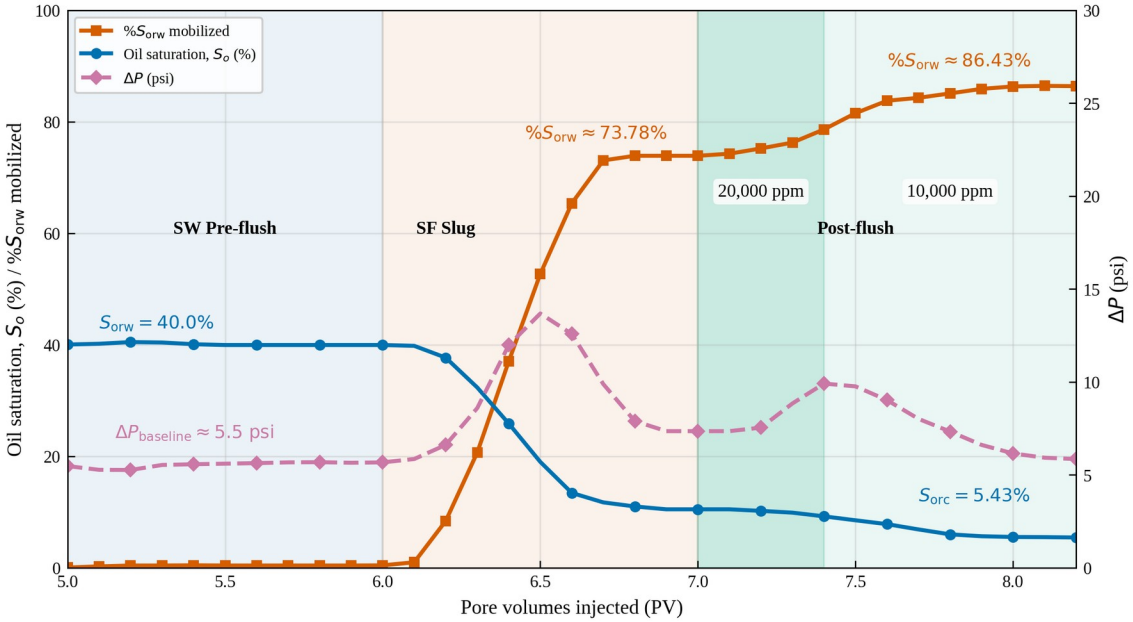

Fig. 7. Dynamic coreflooding response for Core-2 (reservoir carbonate) at 100 °C: oil saturation, tertiary recovery, and differential pressure versus injected PV.

Waterflood and conditioning. The centrifuge established S_{orw} = 40.0 % before chemical injection. Seawater injection provided a baseline pressure response, with baseline differential pressure at 0.25 cm³·min^{-1} averaging 37.9 kPa (5.50 psi). A 5 PV seawater pre-flush conditioned the core to near-seawater salinity before SF4 injection. This laboratory conditioning volume targets near-complete brine replacement in a short core and differs from field pre-flush sizing.

Surfactant slug injection. SF4 was injected at seawater salinity until the oil cut reached zero at 1.0 PV. Oil mobilization began near 6.2 PV injected. Oil saturation decreased from 40.0 to 10.5 % by the end of the slug. Cumulative mobilization during the slug reached 73.8 % of S_{orw}.

Pressure dynamics. Differential pressure peaked at 102.4 kPa (14.85 psi) at 6.51 PV, then declined toward baseline. This transient response is consistent with mobility changes during the salinity-path transition. The return toward baseline indicates no sustained impairment in injectivity over the measured interval. Core-2 reached a peak resistance factor of F_r = 2.75. Because both corefloods share the same flow rate, core cross-section, carrier-phase viscosity, and SF4 IFT, the Core-2 capillary number is essentially identical to Core-1, $N_c \approx 2.0 \times 10^{-3}$, indicating that the difference in displacement efficiency between the two cores is not attributable to a difference in capillary number.

Post-flush. The salinity-gradient post-flush increased total tertiary recovery to 86.4 % of S_{orw} at 8.05 PV. The final oil saturation was S_{orc} = 5.43 %. A secondary pressure peak occurred during the post-flush at 71.5 kPa (10.37 psi), corresponding to F_r = 1.92. This response is consistent with an additional mobilization event along the evolving in-core salinity path.

3.4.3. Bounded interpretation of the Core-1 versus Core-2 contrast

Core-2 achieved a higher displacement efficiency (86.4 % of S_{orw}) than Core-1 (76.1 % of S_{orw}). The dataset does not isolate permeability as the driver of this contrast. Several factors covary between the two cores, including permeability, mineralogy and net adsorption affinity, and initial S_{orw}. Core-2 is tighter (4.42×10^{-3} μm², 4.42 mD) than Core-1 (27.0×10^{-3} μm², 27.0 mD), yet it produced higher tertiary recovery. Static-adsorption screening reported in §3.3.1 indicates a lower net adsorption affinity on the reservoir carbonate (0.78 mg·g^{-1}) than on Indiana limestone (0.87 mg·g^{-1}). Lower adsorption affinity is consistent with reduced surfactant loss at the leading edge of the slug and would preserve more in-core surfactant inventory. The contrast cannot be uniquely assigned to permeability, adsorption affinity, wettability, or S_{orw}, and the interpretation is reported as a bounded mechanistic hypothesis rather than a unique attribution [22].

Both floods used the same endpoint criterion for the SF4 stage: SF4 injection continued until the oil cut reached zero. This endpoint occurred after 1.0 PV in Core-2 and 0.8 PV in Core-1, indicating that the PV-to-zero-oil-cut reflects the specific core response rather than an imposed design variable. Initial S_{orw} was 40.0 % in Core-2 compared with 30.1 % in Core-1. A higher S_{orw} corresponds to a denser population of trapped clusters; upon IFT reduction, this denser population can support coalescence into a continuous oil bank, which is one plausible contributor to higher mobilization efficiency [28]. Normalized chemical utilization also favored Core-2: the recovered oil volume during the SF4 stage corresponds to 0.346 PV oil per PV injected SF4 in Core-2 versus 0.286 PV oil per PV injected SF4 in Core-1. These values reflect gross volumetric utilization based on total injected volume; the effective utilization at the displacement front is lower because of dynamic retention losses.

Ambient chip-scale contact angles shifted from 161° to 69° on Indiana limestone and from 171° to 72° on reservoir carbonate after SF4 exposure. These ambient measurements are qualitative screening indicators and do not establish in-situ wettability at 100 °C and reservoir pressure. The direction of the shift is consistent with reduced capillary trapping. The corefloods demonstrate high microscopic displacement efficiency for SF4 under the tested conditions. These surfactant-only floods do not establish a field-scale sweep. Short cores reduce the heterogeneity length scale and reduce fingering opportunity relative to field conditions. Field-scale sweep requires mobility control [29].

3.4.4. Screening summary

SF4 met the laboratory screening criteria adopted in this study: aqueous and thermal stability under the tested conditions, ultra-low IFT, and low post-flush dynamic retention. It shifted S^* into the seawater-injection window, achieved σ_{os} in the 10^{-3} mN·m^{-1} regime at 100 °C, mobilized 76.1–86.4 % of S_{orw} in surfactant-only floods, and yielded 0.16–0.17 mg·g^{-1} final dynamic retention after the salinity-gradient post-flush. Table 8 consolidates the screening-relevant SF4 metrics used in the subsequent upscaling and screening sections.

Table 8. Consolidated physical and operational parameters of formulation SF4 for field-scale screening.

Metric	Value	Notes
Thermal stability	Stable for 30 days at 120 °C	Seawater matrix
Aqueous stability limit	75 000 ppm TDS at 100 °C	Requires seawater pre-flush
Winsor Type III window	30 000 to 60 000 ppm TDS	At 100 °C
Optimum salinity, S^*	46 000 ppm TDS	At 100 °C
Characteristic solubilization ratio, R^*	12.0 cm^3·cm^{-3}	At S^*
IFT at S^* from Huh correlation, σ^*	2.08×10^{-3} mN·m^{-1}	Eq. (3)
IFT at seawater salinity at 100 °C, σ_{os}	1.93×10^{-3} mN·m^{-1}	Fig. 4 extrapolation
Contact-angle shift, Indiana limestone	161° to 69°	Ambient qualitative indicator
Contact-angle shift, reservoir carbonate	171° to 72°	Ambient qualitative indicator
Coreflood recovery, Core-1	76.1 % of S_{orw}	0.8 PV to zero oil cut
Coreflood recovery, Core-2	86.4 % of S_{orw}	1.0 PV to zero oil cut
Final dynamic retention, Core-1	0.16 mg·g^{-1}	After salinity-gradient post-flush
Final dynamic retention, Core-2	0.17 mg·g^{-1}	After salinity-gradient post-flush

3.5. Positioning against published GAC and IOS carbonate corefloods

Table 9 benchmarks the two SF4 surfactant-only corefloods against published GAC and IOS carbonate corefloods. The table reports permeability, temperature, formation-water salinity, chemical-slug salinity, process type, S_{orw}-normalized recovery, and dynamic retention (Γ) as reported by each source. The discussion focuses on four screening drivers: permeability and rock representativeness, process complexity, temperature envelope, and Γ reporting and magnitude. Cross-study comparison includes differences in crude oil, wettability state, slug size, and salinity path. The benchmark isolates the joint challenge of low permeability, 100 °C operation, surfactant-only simplicity, and reported dynamic retention.

Table 9. Comparison of SF4 dynamic-coreflooding performance against published GAC and IOS-based evaluations in carbonate lithologies.

Reference	Rock type	k / 10^{-3} µm^2	T (°C)	FW salinity (ppm)	Chem. slug salinity (ppm)	Process	Recovery of S_{orw} (%)	Γ (mg·g^{-1})
Lu et al. [15]	Reservoir carbonate	6	100	116 969	57 251	Surfactant only	66.0	0.086
Lu et al. [11]	Silurian dolomite	478	100	66 800	36 000	SP	90.5	0.33
Parra et al. [17]	Indiana limestone	11	78	95 000	95 000	Surfactant only	69.4	N/A
Jabbar et al. [16]	Reservoir carbonate	6.3	98	70 063	74 000	SP	92.0	1.00
Al-Murayri et al. [31]	Reservoir carbonate	35	78	49 964	79 964	ASP (hybrid alkali)	84.5	0.51
Maubert et al. [12]	Indiana limestone	373	83	230 000	93 000	ASP (NaOH)	84.5	0.250
Ghosh et al. [30]	Indiana limestone	292	80	90 000	62 500	SP	38.1	N/A
Ghosh et al. [13]	Indiana limestone	275	80	92 336	79 000	SP	90.0	0.27
Abalkhail et al. [14]	Reservoir carbonate	181.7	100	57 539	60 000	ASP (ammonia)	93.6	0.083
Abalkhail et al. [14]	Indiana limestone	173	100	57 539	60 000	ASP (ammonia)	85.2	0.06

Reference	Rock type	k / 10^{-3} μm²	T (°C)	FW salinity (ppm)	Chem. slug salinity (ppm)	Process	Recovery of S_{orw} (%)	Γ (mg·g^{-1})
This work (Core-1)	Indiana limestone	27.0	100	167 301	43 373	Surfactant only	76.1	0.16
This work (Core-2)	Reservoir carbonate	4.42	100	243 028	43 373	Surfactant only	86.4	0.17

Γ is reported as provided in each source. In this work, Γ denotes final dynamic retention after the salinity-gradient post-flush.

3.5.1. Permeability regime and rock representativeness

Many published studies use a high-permeability regime as shown in Table 9. Lu et al. [11] at 478 × 10^{-3} μm², Maubert et al. [12] at 373 × 10^{-3} μm², Ghosh et al. [30] and [13] at 292 and 275 × 10^{-3} μm², and Abalkhail et al. [14] at 173–181.7 × 10^{-3} μm² (values reported as mD in the source studies; 1 mD ≈ 0.987 × 10^{-3} μm² and the equivalence is retained at screening precision throughout this comparison). These permeability levels reduce transport constraints and moderate the surface-area penalty that drives adsorption and retained mass. Tight-carbonate benchmarks remain limited in Table 9. Only three literature cases report permeability at or below 11 × 10^{-3} μm²: Parra et al. [17] at 11 × 10^{-3} μm², Jabbar et al. [16] at 6.3 × 10^{-3} μm², and Lu et al. [15] at 6 × 10^{-3} μm². Core-2 at 4.42 × 10^{-3} μm² extends this tight-rock space in reservoir carbonate.

Lu et al. [15] report a surfactant-only flood at 100 °C in a fractured reservoir carbonate with 6 × 10^{-3} μm² matrix permeability, with 66.0 % recovery of S_{orw} and Γ = 0.086 mg·g^{-1}. Jabbar et al. [16] reported an SP flood in reservoir carbonate at 6.3 × 10^{-3} μm² and 98 °C with 92.0 % recovery of S_{orw} paired with Γ = 1.00 mg·g^{-1}. Core-2 extends this dataset into the sub-5 × 10^{-3} μm² regime, with 86.4 % recovery of S_{orw} at 4.42 × 10^{-3} μm² and 100 °C and Γ = 0.17 mg·g^{-1}. Relative to Lu et al. [15], this represents higher S_{orw}-normalized recovery within the same temperature class, although the comparison remains conditional on differences in rock, crude oil, and salinity path. Relative to Jabbar et al. [16], SF4 reduces Γ from 1.00 to 0.17 mg·g^{-1} while operating in an even tighter reservoir carbonate core. Core-1 supports interpretability across rock classes under the same thermal conditions and seawater-slug salinity, reaching 76.1 % recovery of S_{orw} at 27.0 × 10^{-3} μm² with Γ = 0.16 mg·g^{-1}.

3.5.2. Process simplicity versus SP and ASP dependence

Table 9 indicates that much of the literature relies on SP or ASP designs [11, 12, 14, 16, 31]. These processes support sweep and mobility control; however, they introduce polymer-handling constraints and alkali compatibility requirements. Abalkhail et al. [14] define a high-performance ASP benchmark at 100 °C in a reservoir carbonate core (93.6 % recovery of S_{orw} with Γ = 0.083 mg·g^{-1} at 181.7 × 10^{-3} μm²).

SF4 achieved competitive displacement efficiencies using a surfactant-only process under a more restrictive transport regime. Core-2 reached 86.4 % recovery of S_{orw} at 4.42 × 10^{-3} μm² with Γ = 0.17 mg·g^{-1}. Core-1 reached 76.1 % recovery of S_{orw} at 27.0 × 10^{-3} μm² with Γ = 0.16 mg·g^{-1}. The dataset indicates that SF4 sustains high microscopic displacement efficiency at 100 °C without polymer or alkali, while reporting low retained mass in a tight reservoir carbonate core.

3.5.3. Temperature and seawater-salinity logistics

Five studies within the 78–83 °C temperature range are listed in Table 9 [17, 31, 30, 13, 12]. High-temperature data at 98–100 °C remain sparse in tight cores and surfactant-only designs. Lu et al. [15] provide a key tight-core surfactant-only data point at 100 °C and 6 × 10^{-3} μm². This work includes two additional surfactant-only corefloods at 100 °C, with a reservoir carbonate core at 4.42 × 10^{-3} μm².

This work evaluates SF4 at 100 °C under seawater-slug logistics. The chemical-slug salinity is 43 373 ppm, aligned with seawater injection. Formation-water salinity spans 167 301 to 243 028 ppm. The aqueous stability limit at 100 °C requires seawater pre-flush and explicit salinity-path management during slug propagation. This links laboratory evaluation to a field-translatable seawater-injection pathway rather than an selected laboratory salinity that bypasses in-situ mixing constraints.

3.5.4. Retention reporting and screening relevance

Table 9 shows incomplete dynamic-retention (Γ) reporting in parts of the literature. The Γ column is N/A in Ghosh et al. [30] and Parra et al. [17]. This limits retention-based screening because retained mass directly controls chemical utilization in carbonate reservoirs. This work reports Γ after a salinity-gradient post-flush in both lithologies and pairs these values with S_{orw}-normalized recovery. Core-1 reports Γ = 0.16 mg·g^{-1} with 76.1 % recovery of S_{orw}. Core-2 reports Γ = 0.17 mg·g^{-1} with 86.4 % recovery of S_{orw}. This pairing supplies the core inputs for the retention-controlled screening framework developed in §3.6 and supports early feasibility screening in tight carbonates where retention dominates chemical utilization.

Taken together, Table 9 positions SF4 within the published GAC and IOS carbonate-coreflood dataset for tight reservoir carbonate at 100 °C under seawater-slug constraints, with high S_{orw}-normalized recovery and low retained mass in a surfactant-only process.

3.6. Field translation and retention-controlled screening

This section links surfactant-only laboratory results to field screening under explicit maturity and sweep assumptions. The sweep efficiency E_v represents the contacted rock volume under mobility control and conformance management. E_v is treated as a conditional input dependent on polymer-assisted sweep rather than a measured outcome of the surfactant-only corefloods. The objective is to screen and rank under the stated assumptions; the framework is a screening tool, not a project NPV model.

3.6.1. Volumetric upscaling

Laboratory corefloods report tertiary recovery as a fraction of residual oil saturation after waterflooding (S_{orw}). Field screening requires incremental recovery on an OOIP basis, reported as RF_{inc}. The volumetric upscaling relationship for Core-2 is:

$$RF_{inc} = RF_{lab} \cdot (S_{orw} / S_{oi}) \cdot E_v \quad (8)$$

where RF_{lab} is the laboratory tertiary recovery fraction of S_{orw}, S_{orw}/S_{oi} is the maturity ratio linking remaining oil after waterflooding to initial oil saturation, and E_v is the field volumetric sweep efficiency. This work upscales Core-2 only because it uses a reservoir carbonate core.

Maturity ratio selection. S_{orw}/S_{oi} represents the fraction of initial oil saturation remaining after waterflooding at the sector scale. Sector-scale initial oil saturations (S_{oi}) of approximately 0.70–0.80 and post-waterflood residual oil saturations (S_{orw}) of about 0.35–0.40 are representative of residual-oil-rich cases relevant to screening. This framing aligns with residual oil saturations reported after waterflooding for Middle East carbonates [32, 33]. Accordingly, $S_{orw}/S_{oi} = 0.50$ was adopted as the base case.

Volumetric sweep efficiency selection. E_v captures the contacted rock volume at the pattern scale and represents a conditional screening assumption tied to polymer-assisted sweep. Without mobility control, E_v declines because of viscous fingering under an adverse mobility ratio. E_v was treated as a literature-informed screening variable rather than as a measured field constant. The cited carbonate literature indicates that contacted volume is limited by heterogeneity, breakthrough, and conformance effects, while polymer and diversion measures may improve sweep relative to an unmanaged flood. Accordingly, $E_v = 0.60$ was adopted to represent moderate sweep outcomes within the same carbonate screening framework rather than a direct field measurement [34, 32].

Base case. The base-case screening values are $RF_{lab} = 0.864$, $S_{orw}/S_{oi} = 0.50$, and $E_v = 0.60$. These yield $RF_{inc} = 25.9$ % OOIP. Fig. S2 in the Supplementary Material maps RF_{inc} as a function of E_v and RF_{lab} at $S_{orw}/S_{oi} = 0.50$. Under fixed $S_{orw}/S_{oi} = 0.50$ and $E_v = 0.60$, Eq. (8) implies a volumetric ceiling of $RF_{inc} \leq 30$ % OOIP even at $RF_{lab} = 1.00$. Near this contour, RF_{inc} is sensitive to E_v.

3.6.2. Retention-cost screening

Retention constrains chemical utilization and screening feasibility in carbonate chemical EOR. A surfactant-retention-cost screening metric C_{ret} quantifies the cost contribution from surfactant mass retained on rock per incremental barrel. C_{ret} is a screening gate on retention only. It prices the surfactant mass retained on the rock after the post-flush material balance, as represented by the dynamic retention Γ. It excludes mobile surfactant in the produced stream, polymer and alkali costs, water handling, and facilities. C_{ret} therefore satisfies a retention-cost screening gate with narrow margin, not a full project cost estimate.

The retention-cost metric is defined as:

$$C_{ret} = (P_s \cdot M_{loss}) / Q_{inc} \quad (9)$$

where $C_{ret,base}$ is in USD per incremental bbl, P_s is the surfactant purchase price in USD·lb^{-1}, M_{loss} is the retained surfactant mass for the chosen basis, and Q_{inc} is the incremental oil produced in bbl. For the base-case definition, $Q_{inc} = 1$ incremental bbl by construction.

To compute $C_{ret,base}$, we convert Γ_{base} to a mass fraction: 0.17 mg·g^{-1} = 1.7 × 10^{-4} lb/lb-rock. For the 1 incremental bbl basis, the base case assumes $RF_{inc,base} = 25.9$ %, giving OOIP = 1/$RF_{inc,base}$ = 3.86 STB. With a formation volume factor $B_o = 1.20$ RB/STB, OOIP in reservoir barrels is OOIP × B_o. Using $S_{oi} = 0.70$, the contact pore volume is PV = (OOIP × B_o)/S_{oi} = 6.62 RB. For porosity $\phi = 0.22$, the contacted bulk rock volume is BRV = PV/ϕ = 30.1 RB, or 168.9 ft^3. Using a bulk density of 132 lb·ft^{-3} yields m_{rock} = 22 300 lb.

The retained surfactant mass per incremental bbl is $M_{loss} = \Gamma_{base} \times m_{rock} = 3.79$ lb per incremental bbl. With $P_{s,base} = 1.50$ USD·lb^{-1}, $C_{ret,base} \approx$ 5.69 USD per incremental bbl. A scaling relationship is used to screen retention cost away from the base case:

$$C_{ret}(\Gamma) = C_{ret,base} \cdot (\Gamma / \Gamma_{base}) \quad (10)$$

Retention budget and limits. A retention budget B (USD per incremental bbl) defines an economic limit for retention-controlled screening. This work uses $B_{max} = 6$ USD per incremental bbl as an upper-limit gate for the retention-penalty term C_{ret} and $B_{pref} = 4$ USD per incremental bbl as a preferred early screen. Published SP/ASP cost benchmarks vary with facilities scope, slug design, and procurement basis [9, 35, 36, 37]. C_{ret} excludes mobile chemical mass and non-chemical field costs. B_{max} therefore constrains the retained-surfactant penalty to a minority share of a viable chemical budget. Under the base case ($P_{s,base} = 1.50$ USD·lb^{-1}, $\Gamma_{base} = 0.17$ mg·g^{-1}, $RF_{inc} = 25.9$ % OOIP), B_{max} corresponds to $\Gamma_{max} \approx 0.18$ mg·g^{-1}. B_{pref} corresponds to $\Gamma \approx 0.12$ mg·g^{-1} under the same assumptions. These limits align with the retention target band of 0.1–0.2 mg·g^{-1} reported for ASP processes [8]. The budget B is converted to a maximum allowable retention Γ_{max} by inverting Eq. (9):

$$\Gamma_{max} = (B \cdot \Gamma_{base}) / C_{ret,base} \quad (11)$$

Surfactant price. The base case uses $P_{s,base} = 1.50$ USD·lb^{-1}, consistent with regional bulk-procurement screening estimates [31]. Sensitivity bounds of $P_s = 1.00$–2.50 USD·lb^{-1} are evaluated in Fig. 8. The base-case price implies $\Gamma_{max} = 0.179$ mg·g^{-1}. The intersection of the base case marker with the B = 6 USD curve indicates that the screened formulation ($\Gamma = 0.17$ mg·g^{-1}) lies within the feasible economic window, with narrow margin if E_v degrades or P_s increases. At fixed RF_{inc}, increases in Γ or reductions in E_v move conditions toward the screening boundary, which motivates adsorption control through salinity management and pre-flush design.

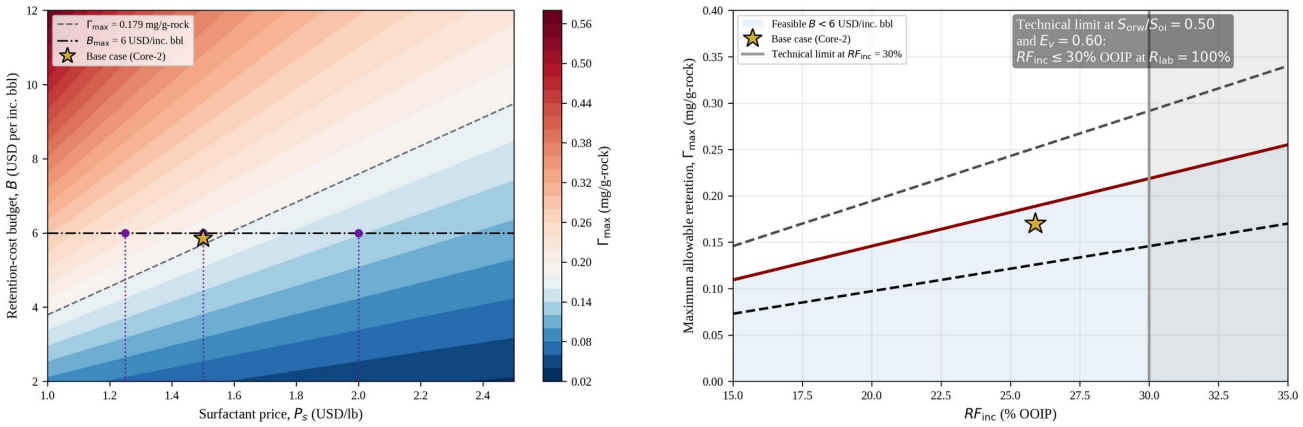

Fig. 8. Maximum allowable retention Γ_{max} for Core-2 satisfying the retention-cost budget B (Eq. (11)): (a) Γ_{max} versus surfactant price P_s and budget B at fixed RF_{inc} = 25.9 % OOIP; (b) Γ_{max} versus RF_{inc} at $P_s = P_{s,base}$ = 1.50 USD·lb^{-1} for budgets B = 4, 6, and 8 USD per incremental bbl.

3.6.3. Retention reduction as the dominant lever

Retention Γ drives C_{ret} linearly through Eq. (9); retention reduction is therefore the dominant lever for expanding screening margin and lowering unit technical cost. Fig. 9 presents an illustrative unit-technical-cost (UTC) waterfall at an oil price of 60 USD/bbl, decomposing the per-incremental-bbl cost into facilities CAPEX, OPEX, chemical spend, and the retained-mass penalty embedded in C_{ret}. The retained-mass term is the single largest chemical contributor in the base case (Γ_{base} = 0.17 mg·g^{-1}; $C_{ret,base}$ = 5.69 USD/bbl). Lowering retention toward Γ = 0.10 mg·g^{-1} reduces C_{ret} to 3.35 USD/bbl through Eq. (10), freeing 2.34 USD/bbl inside the retention budget. As an order-of-magnitude scale, a 0.30 PV alkali-assisted slug at 1 wt % alkali corresponds to approximately 1 USD/bbl of additional chemical spend under the same volumetric scaling, leaving a net benefit before water-treatment and operational impacts [9, 37]. Full UTC stack composition, price-deck assumptions, and sensitivity tornadoes are provided in the Supplementary Material §S1 [38, 39, 40, 41].

Fig. 9. Illustrative unit-technical-cost (UTC) breakdown at an oil price of 60 USD/bbl, reported per incremental bbl. (Detailed UTC stack and price-deck assumptions are in the Supplementary Material.)

3.6.4. Field-translation risk envelope

Sensitivity plots translate the retention budget into a field-screening envelope. Fig. 10 consolidates retention screening in two spaces: (a) C_{ret} as a function of E_v and Γ at $P_s = P_{s,base}$, and (b) C_{ret} as a function of P_s and Γ at fixed E_v = 0.60. The retention-cost screening links two coupled levers: Γ sets C_{ret} at fixed P_s, while E_v sets RF_{inc} and shifts the iso-cost contours. SF4 sits inside the feasible region for B_{max} = 6 USD per incremental bbl, yet lies near the boundary. The position supports feasibility but demands retention reduction to protect against field variability. Strategies that reduce Γ widen the margin without requiring higher E_v.

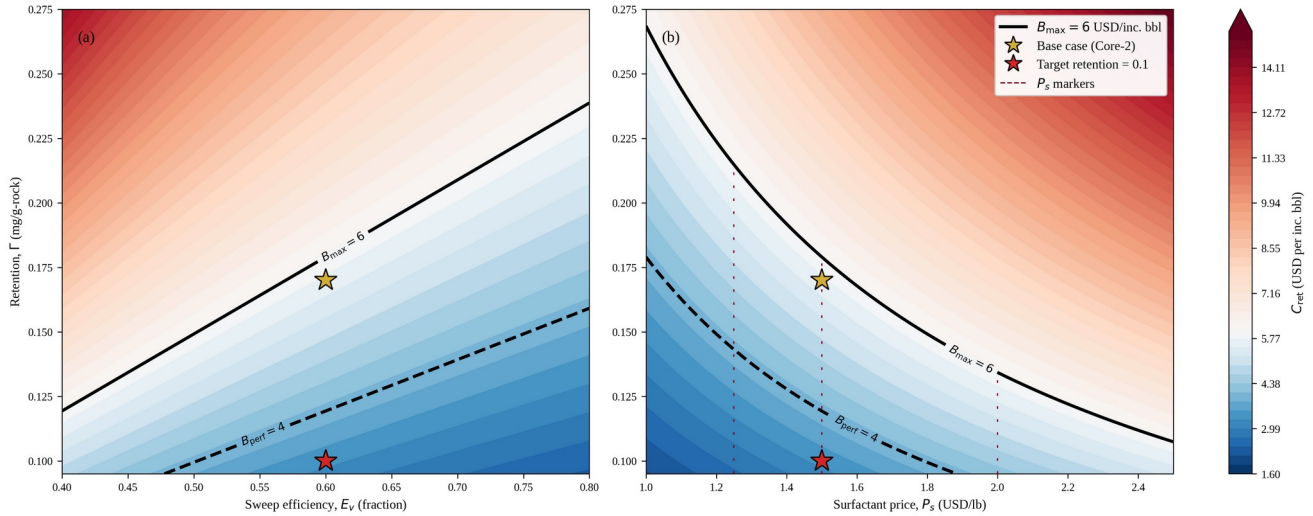

Fig. 10. Retention-cost screening C_{ret} for Core-2 under B = 6 USD per incremental bbl: (a) C_{ret} as a function of E_v and Γ at $P_{s,base}$ = 1.50 USD·lb^{-1} and S_{orw}/S_{oi} = 0.50; (b) C_{ret} as a function of P_s and Γ at fixed E_v = 0.60.

4. Field-development implications and research priorities

4.1. Operational levers

4.1.1. Retention reduction

Retention Γ drives C_{ret} linearly, so retention reduction is a primary lever for expanding feasibility margin. Future investigations should evaluate pathways that push Γ toward 0.10 mg·g^{-1} in HTHS carbonates. Candidate strategies include sacrificial agents that pre-occupy adsorption sites, adsorption suppressors compatible with high salinity, and carbonate-tolerant hybrid alkali systems designed to reduce surface-charge-driven adsorption while controlling scaling risk. These strategies should be integrated with brine-path design — softened brine, ion engineering, and tuned pre-flush sizing — to quantify each option by incremental Γ reduction and the net change in the UTC stack.

4.1.2. Mobility control and sweep protection

Sweep efficiency E_v controls incremental recovery factor and therefore controls retention cost inversely through the RF_{inc} denominator. For S_{orw}/S_{oi} = 0.50, RF_{inc} decreases from 25.9 % OOIP at E_v = 0.60 to 17.3 % OOIP at E_v = 0.40. This increases retention cost from 5.69 to 8.52 USD per barrel at Γ = 0.17 mg·g^{-1}. Attaining E_v near 0.60 requires polymer-based mobility control and conformance management.

4.1.3. Operational constraints affecting field translation

Aqueous stability sets an operational constraint on salinity management. The 75 000 ppm aqueous stability limit at 100 °C is far below formation-water salinity. Field translation therefore requires a seawater pre-flush. The management of the mixing zone between the formation water and the chemical slug controls the precipitation risk. Dispersive mixing elevates local salinity above the stability boundary at the leading edge of the chemical slug and triggers precipitation if it crosses the aqueous stability limit. This risk must be mitigated through robust slug sizing or salinity-gradient design.

Retention shows the same operational sensitivity. Field-scale Γ can increase when the in-situ salinity path deviates from the laboratory design because of mixing, heterogeneous mineralogy, variable residence time, and scale-control chemistry. For pilot evaluation, Γ is treated as a distribution rather than a point estimate. Mitigation designs should aim to shift the expected retention value and reduce variance to maintain operational margins below the screening ceiling.

4.2. Pilot-readiness research priorities

4.2.1. HTHS mobility-control integration

Subsequent research should incorporate polymer screening under 100 °C and representative salinity and hardness, followed by surfactant–polymer floods to evaluate mobility control. These investigations must quantify polymer injectivity, retention, and permeability reduction in the same reservoir carbonate. Polymer chemistry and stability at high temperature remain key barriers to field translation.

4.2.2. Microemulsion rheology and in-situ phase behavior

The Core-2 flood exhibited primary and secondary pressure peaks. This response is consistent with evolving in-core phase behavior and bank properties along the salinity path. Direct measurement of microemulsion viscosity and phase continuity under controlled salinity trajectories will strengthen mechanistic closure and support injection design [42].

4.2.3. Expanded reservoir evaluation and transport-based upscaling

Additional reservoir corefloods across a range of permeabilities, facies, and wettability states will bound uncertainty. A transport model with dispersion and retention parameters tied to effluent histories will improve field-scale prediction of retention and salinity-gradient performance. Tracer tests under the same thermal and salinity conditions will strengthen dispersion parameterization for the transport model.

5. Conclusions

This study developed a retention-controlled screening framework that links laboratory formulation performance to field-translatable incremental recovery in HTHS carbonate reservoirs, and applied the framework to a surfactant-only GAC/IOS blend (designated SF4) designed for seawater injection at 100 °C. Key conclusions are:

(1) The screening framework integrates stability, phase behavior, IFT, retention, and surfactant-only coreflooding, and gates field translation through a surfactant-retention-cost metric C_{ret} under an upper retention budget B_{max}.

(2) SF4 (1.0 wt % active GAC/IOS in seawater, 0.5 wt % co-solvent) was thermally stable for 30 days at 120 °C, formed a Winsor III window from 30 000 to 60 000 ppm with $S^* = 46\,000$ ppm, and gave $\sigma_{os} = 1.93 \times 10^{-3}$ mN·m^{-1} at 100 °C at seawater salinity.

(3) Surfactant-only corefloods at 100 °C mobilized 76.1 % of S_{orw} in outcrop Indiana limestone ($k_w = 27.0 \times 10^{-3}$ μm^2) and 86.4 % of S_{orw} in reservoir carbonate ($k_w = 4.42 \times 10^{-3}$ μm^2). Final dynamic retention after a salinity-gradient post-flush was 0.16–0.17 mg·g^{-1}.

(4) The aqueous stability limit of 75 000 ppm at 100 °C is below formation salinity, so seawater pre-flush and explicit salinity-path management are required for field translation.

(5) Field screening for Core-2 under $S_{orw}/S_{oi} = 0.50$ and $E_v = 0.60$ yields $RF_{inc} = 25.9$ % OOIP and $C_{ret} = 5.69$ USD per incremental bbl, satisfying the retention-cost screening gate $B_{max} = 6$ USD per incremental bbl with narrow margin.

(6) Retention reduction toward 0.10 mg·g^{-1} is the dominant field-translation lever and the principal target for subsequent research; the framework is transferable to analogous HTHS carbonate development settings.

Nomenclature

Symbols

B	**Screening retention-cost budget (USD per incremental bbl)**
B_o	Formation volume factor (RB/STB)
C_0	Injected surfactant concentration in aqueous phase (ppm as mg·L^{-1})
C_{eff}	Effluent surfactant concentration during coreflood (ppm as mg·L^{-1})
C_{eq}	Equilibrium surfactant concentration in static-adsorption supernatant (ppm as mg·L^{-1})
C_{Huh}	Huh-correlation constant (mN·m^{-1})
C_{ret}	Retention cost (USD per incremental bbl)
$C_{ret,base}$	Base-case retention cost (USD per incremental bbl)
E_v	Volumetric sweep efficiency (fraction)
F_r	Resistance factor ($\Delta P/\Delta P_{baseline}$)
k_w	Absolute water permeability (× 10^{-3} μm^2 or mD)
$k_{w,Sorw}$	Effective permeability to water at residual oil saturation (× 10^{-3} μm^2 or mD)
m_{rock}	Dry rock mass of core plug or contacted rock volume (g or lb)
M_{loss}	Retained surfactant mass per Q_{inc} (lb per incremental bbl)
N_c	Capillary number (dimensionless)
P_s	Surfactant price, active basis (USD·lb^{-1})
$P_{s,base}$	Base-case surfactant price (USD·lb^{-1})
Q_{inc}	Incremental oil volume basis used for screening (bbl)
R^*	Characteristic solubilization ratio at optimum salinity
RF_{inc}	Incremental recovery factor on an OOIP basis (% OOIP)
$RF_{inc,base}$	Base-case incremental recovery factor (% OOIP)

RF_{lab}	Laboratory recovery fraction of S_{orw}
R_e	Reynolds number (dimensionless)
R_o	Oil solubilization ratio (V_o/V_s)
R_w	Water solubilization ratio (V_w/V_s)
S^*	Optimum salinity (ppm or wt %)
S_{oi}	Initial oil saturation (fraction)
S_{orc}	Residual oil saturation after chemical flood (fraction)
S_{orw}	Residual oil saturation after waterflood (fraction)
S_{wi}	Initial water saturation (fraction)
V	Solution volume (mL or L)
V_{inj}	Injected aqueous volume used in dynamic-retention balance (mL or L)
V_o	Oil volume in solubilization test (mL)
V_s	Volume of active surfactant solubilized in the middle phase (mL)
V_w	Water/brine volume in solubilization test (mL)

Greek letters

Γ	**Dynamic retention (mg·g^{-1})**
Γ_{base}	Base-case dynamic retention (mg·g^{-1})
Γ_{max}	Maximum allowable retention satisfying budget B (mg·g^{-1})
Γ_s	Static adsorption at equilibrium (mg·g^{-1})
ΔP	Differential pressure (kPa or psi)
$\Delta P_{baseline}$	Baseline differential pressure during seawater injection (kPa or psi)
θ	Contact angle (°)
μ	Viscosity (mPa·s)
ρ	Density (g·cm^{-3})
σ	Interfacial tension (mN·m^{-1})
σ^*	Interfacial tension at optimum salinity (mN·m^{-1})
σ_{os}	Crude-oil–surfactant IFT at seawater salinity (mN·m^{-1})
ϕ	Porosity (fraction)

Abbreviations

API	**American Petroleum Institute (gravity, degrees API)**
ASP	Alkaline–surfactant–polymer
BRV	Bulk rock volume (ft^3 or RB)
CEOR	Chemical enhanced oil recovery
ELSD	Evaporative light-scattering detector
EOR	Enhanced oil recovery
FW	Formation water
GAC	Guerbet alkoxy carboxylate
HPHT	High-pressure, high-temperature
HPLC	High-performance liquid chromatography
HTHS	High-temperature, high-salinity
IFT	Interfacial tension
IOS	Internal olefin sulfonate
NPV	Net present value
OOIP	Original oil in place
PV	Pore volume
SP	Surfactant–polymer
SW	Seawater
TDS	Total dissolved solids
UTC	Unit technical cost

Data Availability

The supplementary-figures document (Figs. S1–S3), the economic-model input workbook, the generated output workbook, and the figure-generation code are provided as Supplementary Material; additional source data are available from the corresponding author on reasonable request.

Declaration of Competing Interest

The authors declare that they have no known competing financial interests or personal relationships that could have appeared to influence the work reported in this paper.

Acknowledgments

The authors acknowledge Abu Dhabi National Oil Company for funding this research under award 8434000317 and Khalifa University of Science and Technology for financial support through the RICH Center (project RC2-2019-007).

References

[1] KAMAL M S, HUSSEIN I A, SULTAN A S. Review on surfactant flooding: Phase behavior, retention, IFT, and tertiary oil recovery. Energy & Fuels, 2017, 31(8): 7701-7720. DOI: 10.1021/acs.energyfuels.7b00353.

[2] SONG Xinmin, LI Yong. Optimum development options and strategies for water injection development of carbonate reservoirs in the Middle East. Petroleum Exploration and Development, 2018, 45(4): 679-689. DOI: 10.1016/S1876-3804(18)30074-0.

[3] WANG Jun, GUO Rui, ZHAO Limin, et al. Geological features of grain bank reservoirs and the main controlling factors: A case study on Cretaceous Mishrif Formation, Halfaya Oilfield, Iraq. Petroleum Exploration and Development, 2016, 43(3): 367-377. DOI: 10.11698/PED.2016.03.06.

[4] GREEN D W, WILLHITE G P. Enhanced oil recovery. SPE Textbook Series. Richardson, Texas, USA: Society of Petroleum Engineers, 2018. DOI: 10.2118/9781613994948.

[5] HIRASAKI G J, MILLER C A, PUERTO M. Recent advances in surfactant EOR. SPE Journal, 2011, 16(4): 889-907. DOI: 10.2118/115386-PA.

[6] ANDERSON W G. Wettability literature survey. Part 6: The effects of wettability on waterflooding. Journal of Petroleum Technology, 1987, 39(12): 1605-1622. DOI: 10.2118/16471-PA.

[7] ADKINS S, LIYANAGE P J, PINNAWALA ARACHCHILAGE G W P, et al. A new process for manufacturing and stabilizing high-performance EOR surfactants at low cost for high-temperature, high-salinity oil reservoirs. SPE-129923-MS, presented at the SPE Improved Oil Recovery Symposium, Tulsa, Oklahoma, USA, 24-28 April, 2010. DOI: 10.2118/129923-MS.

[8] LIU S, LI R F, MILLER C A, et al. ASP processes: Wide range of conditions for good recovery. SPE-113936-MS, presented at the SPE/DOE Improved Oil Recovery Symposium, Tulsa, Oklahoma, USA, 19-23 April, 2008. DOI: 10.2118/113936-MS.

[9] SHENG J J. Critical review of alkaline-surfactant-polymer (ASP) flooding. Asia-Pacific Journal of Chemical Engineering, 2014, 9(4): 471-489. DOI: 10.1002/apj.1824.

[10] ADKINS S, PINNAWALA ARACHCHILAGE G W P, SOLAIRAJ S, et al. Development of thermally and chemically stable large-hydrophobe alkoxy carboxylate surfactants. SPE-154256-MS, presented at the SPE Improved Oil Recovery Symposium, Tulsa, Oklahoma, USA, 14-18 April, 2012. DOI: 10.2118/154256-MS.

[11] LU J, BRITTON C, SOLAIRAJ S, et al. Novel large-hydrophobe alkoxy carboxylate surfactants for enhanced oil recovery. SPE Journal, 2014, 19(6): 1024-1034. DOI: 10.2118/154261-PA.

[12] MAUBERT M, LIYANAGE P J, POPE G A, et al. ASP experiments in Indiana limestone using NaOH to reduce surfactant retention. SPE-190187-MS, presented at the SPE Improved Oil Recovery Conference, Tulsa, Oklahoma, USA, 14-18 April, 2018. DOI: 10.2118/190187-MS.

[13] GHOSH P, SHARMA H, MOHANTY K K. ASP flooding in tight carbonate rocks. Fuel, 2019, 241: 653-668. DOI: 10.1016/j.fuel.2018.12.041.

[14] ABALKHAIL N A, LIYANAGE P J, UPAMALI K A N, et al. Alkaline-surfactant-polymer formulation development for a HTHS carbonate reservoir. Journal of Petroleum Science and Engineering, 2020, 191: 107236. DOI: 10.1016/j.petrol.2020.107236.

[15] LU J, GOUDARZI A, CHEN P, et al. Surfactant enhanced oil recovery from naturally fractured reservoirs. SPE-159979-MS, presented at the SPE Annual Technical Conference and Exhibition, San Antonio, Texas, USA, 8-10 October, 2012. DOI: 10.2118/159979-MS.

[16] JABBAR M Y, AL SOWAIDI A, AL OBEIDLI A, et al. Chemical formulation design in high salinity, high temperature carbonate reservoir for a super giant offshore field in Middle East. SPE-188604-MS, presented at the Abu Dhabi International Petroleum Exhibition and Conference, 13-16 November, 2017. DOI: 10.2118/188604-MS.

[17] PARRA J E, POPE G A, MEJIA M, et al. New approach for using surfactants to enhance oil recovery from naturally fractured oil-wet carbonate reservoirs. SPE-181713-MS, presented at the SPE Annual Technical Conference and Exhibition, Dubai, UAE, 26-28 September, 2016. DOI: 10.2118/181713-MS.

[18] LEVITT D, KLIMENKO A, JOUENNE S, et al. Designing and injecting a chemical formulation for a successful off-shore chemical EOR pilot in a high-temperature, high-salinity, low-permeability carbonate field. SPE-179679-MS, presented at the SPE Improved Oil Recovery Conference, Tulsa, Oklahoma, USA, 11-13 April, 2016. DOI: 10.2118/179679-MS.

[19] VONNEGUT B. Rotational methods for the study of interfacial tension. Review of Scientific Instruments, 1942, 13(1): 6-9. DOI: 10.1063/1.1769937.

[20] HUH C. Interfacial tensions and solubilizing ability of a microemulsion phase that coexists with oil and brine. Journal of Colloid and Interface Science, 1979, 71(2): 408-426. DOI: 10.1016/0021-9797(79)90249-2.

[21] SOLAIRAJ S, BRITTON C, KIM D H, et al. Measurement and analysis of surfactant retention. SPE-154247-MS, presented at the SPE Improved Oil Recovery Symposium, Tulsa, Oklahoma, USA, 14-18 April, 2012. DOI: 10.2118/154247-MS.

[22] PANTHI K, MOHANTY K K. Development of surfactant formulation for high-temperature off-shore carbonate reservoirs. Frontiers in Chemistry, 2024, 12: 1408115. DOI: 10.3389/fchem.2024.1408115.

[23] ANDERSON W G. Wettability literature survey. Part 1: Rock/oil/brine interactions and the effects of core handling on wettability. Journal of Petroleum Technology, 1986, 38(10): 1125-1144. DOI: 10.2118/13932-PA.

[24] ESFANDYARI H, MOGHANI A, ESMAEILZADEH F, et al. A laboratory approach to measure carbonate rocks' adsorption density by surfactant and polymer. Mathematical Problems in Engineering, 2021, 2021: 5539245. DOI: 10.1155/2021/5539245.

[25] BELLO A, IVANOVA A, BAKULIN D, et al. A static and dynamic analysis of nonionic-based binary surfactant systems for adsorption mitigation in a carbonate reservoir with high salinity. Journal of Molecular Liquids, 2024, 407: 125141. DOI: 10.1016/j.molliq.2024.125141.

[26] SHAKEEL M, SAMANOVA A, POURAFSHARY P, et al. Optimization of low salinity water surfactant flooding design for oil-wet carbonate reservoirs by introducing a negative salinity gradient. Energies, 2022, 15(24): 9400. DOI: 10.3390/en15249400.

[27] HIRASAKI G J, VAN DOMSELAAR H R, NELSON R C. Evaluation of the salinity gradient concept in surfactant flooding. SPE Journal, 1983, 23(3): 486-500. DOI: 10.2118/8825-PA.

[28] WANG J, HU Y, CHU X, et al. Roles and thresholds of viscosity and interfacial tension in surfactant flooding for residual oil recovery. Frontiers in Chemistry, 2025, 13: 1660041. DOI: 10.3389/fchem.2025.1660041.

[29] LOHNE A, FJELDE I. Surfactant flooding in heterogeneous formations. SPE-154178-MS, presented at the SPE Improved Oil Recovery Symposium, Tulsa, Oklahoma, USA, 14-18 April, 2012. DOI: 10.2118/154178-MS.

[30] GHOSH P, SHARMA H, MOHANTY K K. Development of surfactant-polymer SP processes for high temperature and high salinity carbonate reservoirs. SPE-191733-MS, presented at the SPE Annual Technical Conference and Exhibition, Dallas, Texas, USA, 24-26 September, 2018. DOI: 10.2118/191733-MS.

[31] AL-MURAYRI M T, KAMAL D S, SUNIGA P, et al. Improving ASP performance in carbonate reservoir rocks using hybrid-alkali. SPE-187213-MS, presented at the SPE Annual Technical Conference and Exhibition, San Antonio, Texas, USA, 9-11 October, 2017. DOI: 10.2118/187213-MS.

[32] OKASHA T M, FUNK J J, ROSHELLE H N. Fifty years of wettability measurements in the Arab-D carbonate reservoir. SPE-105114-MS, presented at the SPE Middle East Oil & Gas Show and Conference, Manama, Bahrain, 11-14 March, 2007. DOI: 10.2118/105114-MS.

[33] AL-MURAYRI M T, HASSAN A A, AL-MAHMEED N, et al. Surfactant/polymer flooding: Chemical-formulation design and evaluation for Raudhatain Lower Burgan Reservoir, Kuwait. SPE Reservoir Evaluation and Engineering, 2019, 22(3): 923-940. DOI: 10.2118/183933-PA.

[34] HENTHORNE L, POPE G A, WEERASOORIYA U P, et al. Impact of water softening on chemical enhanced oil recovery project economics. SPE-169165-MS, presented at the SPE Improved Oil Recovery Symposium, Tulsa, Oklahoma, USA, 12-16 April, 2014. DOI: 10.2118/169165-MS.

[35] SUN Q, ERTEKIN T, ZHANG M, et al. A comprehensive techno-economic assessment of alkali-surfactant-polymer flooding processes using data-driven approaches. Energy Reports, 2021, 7: 2681-2702. DOI: 10.1016/j.egyr.2021.05.003.

[36] WALSH J M, HENTHORNE L. Challenges of water treating for chemical enhanced oil recovery. Oil and Gas Facilities, 2012, 1(4): 9-14. DOI: 10.2118/157531-PA.

[37] TACKIE-OTOO B N, OTCHERE D A, ABDUL LATIFF A H, et al. Evaluation of the oil recovery potential and cost implication analysis of alternative ASP formulations for sandstone and carbonate reservoirs. ACS Omega, 2024, 9(19): 20859-20875. DOI: 10.1021/acsomega.3c09590.

[38] AL-MURAYRI M T, SULAIMAN D S, HASSAN A A, et al. Encouraging chemical EOR field results. SPE-211449-MS, presented at the SPE Annual Technical Conference and Exhibition, 31 October - 2 November, 2022. DOI: 10.2118/211449-MS.

[39] LIU Y, PI J, TONG K. Pore-scale experimental investigation of oil recovery enhancement in oil-wet carbonates at different injection rates. Processes, 2023, 11(8): 2289. DOI: 10.3390/pr11082289.

[40] HAYAVI M T, KAZEMZADEH Y, RIAZI M. Application of surfactant-based enhanced oil recovery in carbonate reservoirs: A critical review of the opportunities and challenges. Chemical Physics Letters, 2022, 802: 139975. DOI: 10.1016/j.cplett.2022.139975.

[41] AITKULOV A, MOHANTY K K. Timing of ASP injection for viscous oil recovery. SPE-179606-MS, presented at the SPE Improved Oil Recovery Conference, Tulsa, Oklahoma, USA, 11-13 April, 2016. DOI: 10.2118/179606-MS.

[42] TAGAVIFAR M, HERATH S, WEERASOORIYA U P, et al. Measurement of microemulsion viscosity and its implications for chemical enhanced oil recovery. SPE Journal, 2018, 23(1): 66-83. DOI: 10.2118/179672-PA.